Acta Mech. Sin. (2017) 33(4):823–832
DOI 10.1007/s10409-017-0674-7

RESEARCH PAPER

Flow dynamics analyses of pathophysiological liver lobules using porous media theory

Jinrong Hu[1,2] · **Shouqin Lü**[1,2] · **Shiliang Feng**[1] · **Mian Long**[1,2]

Received: 3 February 2017 / Revised: 18 March 2017 / Accepted: 1 April 2017 / Published online: 17 May 2017

Abstract Blood flow inside the liver plays a key role in hepatic functions, and abnormal hemodynamics are highly correlated with liver diseases. To date, the flow field in an elementary building block of the organ, the liver lobule, is difficult to determine experimentally in humans due to its complicated structure, with radially branched microvasculature and the technical difficulties that derive from its geometric constraints. Here we established a set of 3D computational models for a liver lobule using porous media theory and analyzed its flow dynamics in normal, fibrotic, and cirrhotic lobules. Our simulations indicated that those approximations of ordinary flow in portal tracts (PTs) and the central vein, and of porous media flow in the sinusoidal network, were reasonable only for normal or fibrotic lobules. Models modified with high resistance in PTs and collateral vessels inside sinusoids were able to describe the flow features in cirrhotic lobules. Pressures, average velocities, and volume flow rates were profiled and the predictions compared well with experimental data. This study furthered our understanding of the flow dynamics features of liver lobules and the differences among normal, fibrotic, and cirrhotic lobules.

Keywords Cirrhotic liver · Structural distortion · Portal hypertension · Collateral vessels

✉ Mian Long
mlong@imech.ac.cn

[1] Center of Biomechanics and Bioengineering, Key Laboratory of Microgravity (National Microgravity Laboratory), Beijing Key Laboratory of Engineered Construction and Mechanobiology, Institute of Mechanics, Chinese Academy of Sciences, Beijing 100190, China

[2] School of Engineering Science, University of Chinese Academy of Sciences, Beijing 100049, China

1 Introduction

Hepatic hemodynamics is distinct from those in conventional microcirculation since there is a dual blood supply to the liver originating from both the portal vein and the hepatic artery. At the same time, the existence of permeable liver sinusoidal endothelium enables blood flow to bypass the mainstream into the Disse gap underneath the endothelium. These unique features of blood flow govern liver-specific functions. For example, only under small shear stress can the peripheral leukocytes recruit into the liver sinusoids effectively through intercellular adhesions [1,2]. After a partial hepatectomy, the altered blood flow inside the liver triggers liver regeneration and regulates the perfusion volume of the liver [3]. Patients with cirrhotic livers always suffer from portal hypertension, which is usually caused by high pressure in the portal vein and high resistance in vessels [4–6]. Hence, quantifying the flow characteristics in the liver is key for understanding the function of the liver.

Liver lobules, the elementary anatomical building blocks of the liver organ, are prismatically shaped with three to eight (usually six) edges [7,8]. Portal tracts (PTs), including terminal portal venules and terminal hepatic arterioles, are located at the intersections of these edges. They extend to the interior of the liver lobule so that the blood can eventually drains into the central vein (CV) through discontinuous capillaries, called hepatic sinusoids. Hepatic sinusoid is a kind of specialized capillary with plenty of fenestrae (100-200 nm in size) on liver sinusoidal endothelial cells (LSECs) and numerous sinusoidal gaps (400–500 nm in size) between the adjacent LSECs, rendering the sinusoids highly permeable. Thus, liver lobules are usually treated as typical porous media [9]. Changes in hepatic tissue structure are intimately

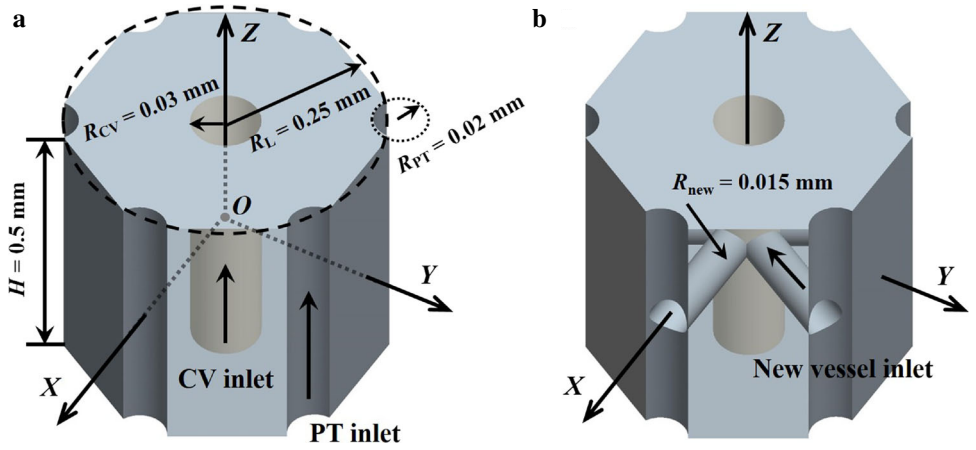

Fig. 1 Geometry of a typical liver lobule for a basic model (**a**) and a model modified by adding the collateral vessels between PTs and CV (**b**)

linked to liver diseases. In the progression of liver fibrosis, a mass of extracellular matrix proteins (such as collagens) accumulate and deposit in the Disse gap; the consequent structural distortion and the disrupted sinusoidal connectivity result in high resistance in the liver [10]. When a fibrotic liver develops into a cirrhotic liver [5], PTs are at a state of high resistance and high pressure along with shunts [6,11], a kind of collateral circulation with the generation of new vessels adjacent to the congested vessels. In this way, liver diseases cause structural distortion and change hemodynamics in the liver, which further aggravates the development of liver diseases in return. Thus, correlating distinct pathophysiological conditions with specified hemodynamics characteristics in the liver is critical in elucidating the underlying mechanisms of liver diseases and their relation to blood flow.

Unfortunately, the aforementioned correlation remains unclear both experimentally and theoretically due to the complexity of liver blood flow. On the one hand, experimental assays used to quantify the bulk flow in the human liver mainly include catheterizing directly [12], nuclear magnetic resonance imaging (MRI) [13] and orthogonal polarization spectral imaging [14,15], all of which focus on monitoring pressure and velocity in trunks. The combination of vascular corrosion casting and micro-CT imaging techniques is able to estimate permeability and porosity of the liver lobule, but it is difficult to conduct quantitative analysis of the flow field [9]. Blood flow in the lobule can be measured more precisely in animals by injecting fluorescent latex microspheres into blood vessels [16] or using micropuncture [17]. To date, good descriptions of the blood flow for the normal human liver in the small-sized lobule and its alterations with the progression of liver diseases development are lacking due to technical difficulties. On the other hand, computational modeling contributes a great deal to predicting the features of this complicated flow. For example, blood flow in a liver lobule is analyzed based on Darcy's law using porous media theory [18,19] or the continuum theory of mixtures [20,21]. It is also effective to build a 3D blood vessel network to mimic the blood flow in liver lobule [22]. Moreover, a few pharmacokinetic models can also provide clues in predicting the flow field for a liver lobule [23–25]. Nevertheless, the theoretical models developed until now are quite limited, and it is hard to take into account diverse pathophysiological cases in vivo, such as fibrotic livers or cirrhotic livers. It is also difficult to directly compare numerical calculations with these few limited measured data.

Here we adopted the porous media theory-based models and verified their validity for flow dynamics in fibrotic or cirrhotic lobules. We further modified these models by assigning high resistance in PTs and adding collateral vessels between PTs and CV to replicate portal hypertension and shunts in the cirrhotic liver. Pressure or velocity profiles and volume flow rates are discussed using the developed 3D computational models, especially in cirrhotic lobules, attempting to further understand the correlation between hepatic hemodynamics and liver diseases.

2 Computational Modeling

2.1 Geometry of a liver lobule model

The 3D hexagonal model of a liver lobule employed in the current work (Fig. 1a) was directly adopted from the literature [19,26], since the geometric dimensions used for modeling liver lobules and the corresponding tracts or vessels have been discussed extensively in those works. Here the lobule was simplified as a hexagonal prism with six cylinders at the ridges to mimic its PTs, and a central cylinder at the center to replicate its CV, both of which serve as the

Table 1 Parameter settings used for liver lobule upon Model B

Physiopathological conditions	Normal	Fibrotic	Cirrhotic	Source
Permeability components (m^2)				
d_{rr}	1.56×10^{-14}	9.87×10^{-14}	5.13×10^{-13}	[9,27]
$d_{\theta\theta}$	1.75×10^{-14}	5.78×10^{-14}	5.63×10^{-13}	[9,27]
d_{zz}	3.64×10^{-14}	1.68×10^{-13}	7.79×10^{-13}	[9,27]
Porosity	0.143	0.143	0.246	[9,27]
Pressure boundary (Pa)				
PT (inlet/outlet)	823.7/690.4	988.4/828.0	1210.8/1014.9	[17,19,28]
CV (inlet/outlet)	679.0/563.0	871.3/704.7	781.0/631.0	[17,19,28]
Volume flow rate ($m^3 \cdot s^{-1}$)	8.80×10^{-13}	2.62×10^{-12}	6.78×10^{-11}	Calculated

channels for blood flow. The height of the regular hexagonal prism $H = 0.5$ mm, and the circumradius of its cross section $R_L = 0.25$ mm. The cylinders located on the six ridges were set as PTs with radius $R_{PT} = 0.02$ mm, and the central cylinder was set as CV with radius $R_{CV} = 0.03$ mm [19,26]. The *grey zone* between the PTs and the CV represents the liver sinusoidal network (Fig. 1), which is permeable in vivo between liver sinusoids and the Disse gap. The geometric model and corresponding meshes were generated by Gambit^{TM}, and the interval size of the mesh was 6 μm [19].

2.2 Physical model

The channels of PTs and the CV were defined as pure fluid zones. The sinusoidal zone was denoted as porous media identified by cell zone conditions in Fluent^{TM}. The governing equation of incompressible fluid flowing through anisotropic porous media is given by Darcy's law,

$$\boldsymbol{v} = -\frac{\boldsymbol{D}}{\mu}\nabla p, \tag{1}$$

where $\boldsymbol{v}$ is the Darcy velocity, μ is the dynamic viscosity, p is the fluid pressure and $\boldsymbol{D}$ is the permeability tensor. When the porous media is isotropic, Eq. (1) becomes:

$$\boldsymbol{v} = -\frac{\boldsymbol{\alpha}}{\mu}\nabla p. \tag{2}$$

Here $\boldsymbol{\alpha}$ is an isotropic permeability tensor, in which its diagonal components are equal and the others are zero. Neglecting thermal effects for purely viscous fluids, the flow field can be obtained theoretically from Eq. (1) or (2) with boundary conditions given below (Table 1).

Two key factors determine blood flow inside the porous media. One is the permeability of the media, which was termed as a symmetric second-order tensor ($\boldsymbol{D}$)

$$\boldsymbol{D} = \begin{pmatrix} d_{rr} & d_{r\theta} & d_{rz} \\ d_{\theta r} & d_{\theta\theta} & d_{\theta z} \\ d_{zr} & d_{z\theta} & d_{zz} \end{pmatrix}. \tag{3}$$

Another parameter, media porosity, was defined as

$$\varepsilon = V_s / V_w, \tag{4}$$

wherein V_s is the blood volume in sinusoids and V_w is the volume of the whole sinusoidal zone. To compare the flow dynamics in physiological and pathological conditions, the values of these two parameters, respectively from normal, fibrotic or cirrhotic lobules, are summarized in Table 1.

2.3 Boundary Conditions

We set the lower terminals of six PTs and one CV as pressure inlets, and the other terminals as pressure outlets [19,22] (Fig. 1a). Here the pressure values for normal human liver were adopted directly from the calculations previously described [19]. Since no clinical data of blood pressures are available for fibrotic and cirrhotic human liver lobules, these pathological values had to be derived from animal studies [17] based on the potential similarity of hemodynamics among mammalian species by assuming that the hemodynamic changes from normal liver to fibrotic or cirrhotic liver are similar between human and other mammalian species [29]. Briefly, we first calculated the blood pressure ratio between normal liver and fibrotic or cirrhotic lobules from murine-based experimental data, and then multiplied the respective ratio by normal human liver pressure to obtain the pressure values of human fibrotic or cirrhotic lobules (Table 1). Notably, while these pressure data from animal studies are not specific for fibrotic lobules but for fatty livers [17], it seemed applicable thanks to the observation that fibrotic lobules and fatty livers are highly correlated [30,31]. In addition, symmetrical boundaries were defined for the six side surfaces, and periodic boundaries were set for both the

Table 2 Modified models for flow analyses of cirrhotic liver lobule

Model	P[a]							V[b]	P+V[c]
	P1	P2	P3	P4	P5	P6	P7		
Permeability (m^2)	1×10^{-2}	1×10^{-8}	1×10^{-10}	1×10^{-11}	1×10^{-12}	1×10^{-13}	5×10^{-14}	N/A	1×10^{-13}

[a] The model that treated the PTs as porous media
[b] The model that added new blood vessels
[c] The combination of models P and V

top and bottom planes. Blood flow in each liver lobule was treated as an incompressible Newtonian fluid with a dynamic viscosity of 3.5 mPa · s and a density of 1050 kg/m^3. This simplified model was named as a basic model (Model B) of a liver lobule with corresponding parameters listed in Table 1, on which flow dynamics analyses were then performed for human normal, fibrotic, and cirrhotic lobules. The flow velocity used here was the physical velocity, but not the superficial velocity applied in the literature [19]. There is a simple formula $v_{\text{superficial}} = \gamma\, v_{\text{physical}}$ (γ is porousity) to define their relationship, and the physical velocity is recommended for more accurate results, as used in the current work.

2.4 Modified models for cirrhotic liver

It is more pathologically relevant to analyze the blood flow in a cirrhotic lobule, since the increase in fibrous matrix and the presence of compensatory circulation significantly distort hepatic hemodynamics [5,6,32,33]. Considering the features of high resistance and multiple shunts in the lobule, we further developed, based on Model B, two other models specific for cirrhotic liver. The first was to set the PT channels as porous media for assigning high resistance in the PTs (designated Model P). This assumption is used to represent typical pathological manifestations of fiber deposition, scar formation, and portal hypertension in cirrhotic liver [5,6]. Here the resistance was varied systematically via setting the distinct permeability values to mimic the progress of liver cirrhosis at different stages. The other was to add six branched vessels in the sinusoid zone at the half-height of the lobule, with their axes along the $x-y$ plane for embodying the feature of multiple shunts (designated Model V) (Fig. 1b). This simplification makes blood bypass the porous, high resistance sinusoids and flow directly from PTs to the CV, which has the effect on releasing portal hypertension or high lobule pressure in cirrhotic liver. The combination of Models P and V, named as Model P+V, was also used for evaluating the cooperative impacts of these two factors on blood flow in cirrhotic liver (Table 2). The same boundary conditions as those in Model B were applied in Models P, V, and P+V.

2.5 Numerical simulations

The simulations in this study were conducted using Fluent™ (Version 15.0). The Porous Zone option in cell zone condition was selected. This is a steady state calculation on incompressible flow through a porous medium by Darcy's law. As a whole, a Newtonian laminar model with viscosity of 3.5 mPa · s was chosen for viscous flow calculations. The SIMPLE algorithm was chosen for pressure-velocity coupling. The default settings of spatial discretization methods, including least squares cell for gradient, second order for pressure, and second order upwind for momentum, were chosen in the simulations. Calculating convergence was defined by obtaining the residual of continuity and velocity $<1 \times 10^{-3}$ or by maintaining the stable residual curve.

3 Results

3.1 Flow dynamics analyses for liver lobule using simplified models

We first investigated the pressure, flow velocity and volume flow rate using Model B for three pathophysiological conditions. Typical pressure profiles at the planes of $Y = 0$ (Fig. 2a, c, e) and $Z = 0$ (Fig. 2b, d, f) showed that the pressure decreased gradually from inlets to outlets, either in PTs or in the CV, as well as from PTs to the CV in normal (Fig. 2a, b), fibrotic (Fig. 2c, d), or cirrhotic (Fig. 2e, f) lobules. However, this pressure reduction damped more slowly in PTs or the CV (Fig. 2e) and more rapidly from PT to the CV in cirrhotic lobules (Fig. 2f), mainly attributed to the higher permeability and porosity as well as the higher pressure boundary (Table 1), as compared to the other two cases. At the current parameter settings, the pressure gradient from PT to the CV typically ranged from 17, 7, 46 Pa along a radical distance of 0.25 mm in normal, fibrotic, and cirrhotic lobules, respectively.

Average bulk velocity within the entire sinusoidal zone and its radical velocity component were also compared among the three cases. For fibrotic lobules, the two values were over six- and two-fold higher than those for normal lobules, respectively. These differences were enlarged when comparing cirrhotic and normal lobules, yielding over twenty-fold higher in bulk velocity and seventy-fold higher in the radical component (Fig. 2g). The flow patterns predicted by our model were qualitatively consistent with those experimental observations for the three cases, implying the

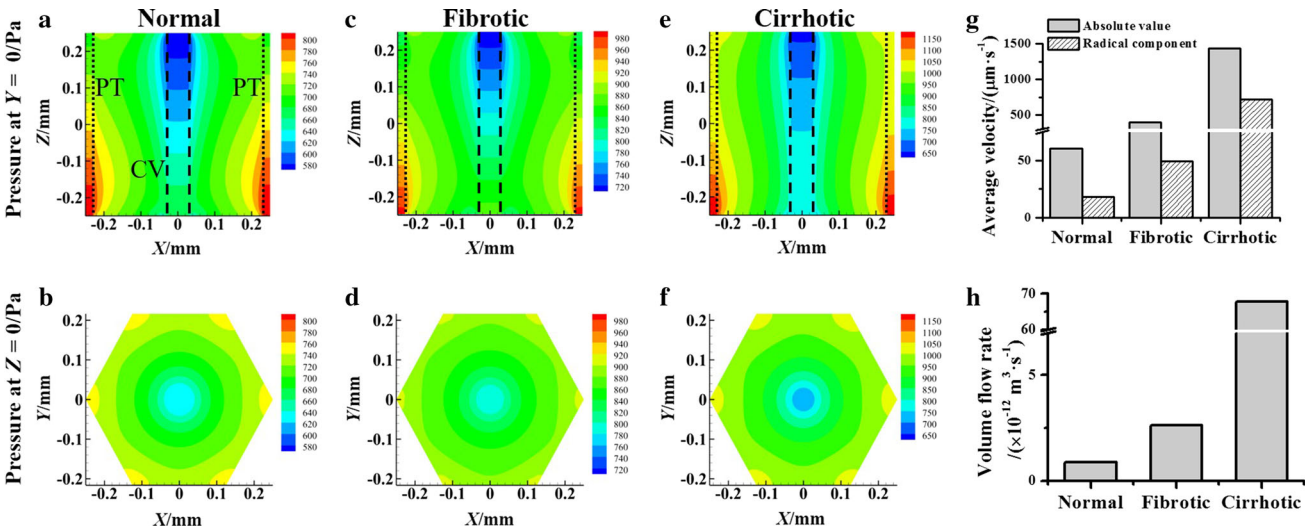

Fig. 2 **a**–**f** Pressure profiles at the planes of $Y = 0$ (**a**, **c**, **e**) and $Z = 0$ (**b**, **d**, **f**) in normal (**a**, **b**), fibrotic (**c**, **d**), and cirrhotic lobule (**e**, **f**) on basic model (Model B). PTs and CV are illustrated as *dotted* and *dashed lines*, respectively. **g**, **h** Average velocities of absolute value and radical component (**g**) and volume flow rate (**h**) in the sinusoidal zone were calculated with different pressure boundary conditions, porosity, and permeability as in Table 1

effectiveness of our modeling. However, the sharp increase of flow velocities in fibrotic or cirrhotic lobules are much higher than those limited data measured in Ref. [16]. Thus, it is required to modify these basic models, as discussed below.

Volume flow rate within the entire sinusoidal zone, referring to the volume of blood flowing through the side wall of the CV per unit time and equal to the flow rate difference between the CV inlet and outlet, is another key indicator to evaluate model validity, as it is one kind of diagnostic criteria for specific liver diseases. Our calculations indicated that the flow rate yielded was 0.88×10^{-12} m$^3 \cdot$ s^{-1} (Table 1) for normal lobules, which was in the same order of magnitude with experimental data estimated from dividing the bulk flow rate of whole liver organ by the number of existing lobules, as discussed below. Again, the flow rate presented a moderate increase of about three-fold in fibrotic lobules and a sharp increase of about eighty-fold in cirrhotic lobules, as compared to those in normal lobules (Fig. 2h).

Taken together, this simplified model was able to map the global features of flow dynamics in liver lobules in the distinct pathophysiological cases. We further tested whether these calculations were in quantitative agreement with experimental data [16]. While the moderate increase of average flow velocity and volume flow rate was reasonable in fibrotic lobules, the sharp enhancement of these two values in cirrhotic lobules did not seem reliable. This implied that this simple Model B, just taking account of the change in permeability and porosity in the sinusoidal network, might not satisfy pathological conditions of cirrhotic lobules when calculating the related flow field.

3.2 Flow dynamics analyses for cirrhotic lobule using modified models

Structural distortion of liver lobules results in high resistance and multiple shunts in the cirrhotic liver. Thus, we modified the simplified model and further developed Model P, Model V, and the combined Model P+V, which could better mimic the key flow characteristics in cirrhotic liver. Here Model P treated the PTs as porous media, but not as ordinary flow in Model B. Model V added six collateral vessels from PTs to the CV. Since lobule resistance enhancement and shunt occurrence vary with the progress of the cirrhotic liver and no experimental data are available, we first tested the effects of PT permeability by systematically varying seven values ranging from 10^{-2} m^2 to 10^{-14} m^2, attempting to find the appropriate value(s) that matched the cirrhotic phenotype. The calculations indicated that the average velocity (Fig. 3a) and volume flow rate (Fig. 3b) exhibited similar values with the permeability above 10^{-10} m^2, followed by a gradual decrease starting from 10^{-11} m^2 to 5×10^{-14} m^2. Assigning porous media in PTs in Model P led to reduced average velocities and volume flow rates compared to those obtained from Model B in cirrhotic lobules (Model B^C) (Fig. 3a, b, *left bars*). Based on the differences in average velocity and volume flow rate between normal and cirrhotic livers from the experimental murine data [16] (Table 3), a specific permeability of 10^{-13} m^2 was chosen for further analyses (Table 2).

Given this permeability value, we tested the changes in pressure profile using the three modified cirrhotic lobule Models P, V, and P+V. High resistance in PTs altered the pressure pattern in Model P in contrast to those in Model

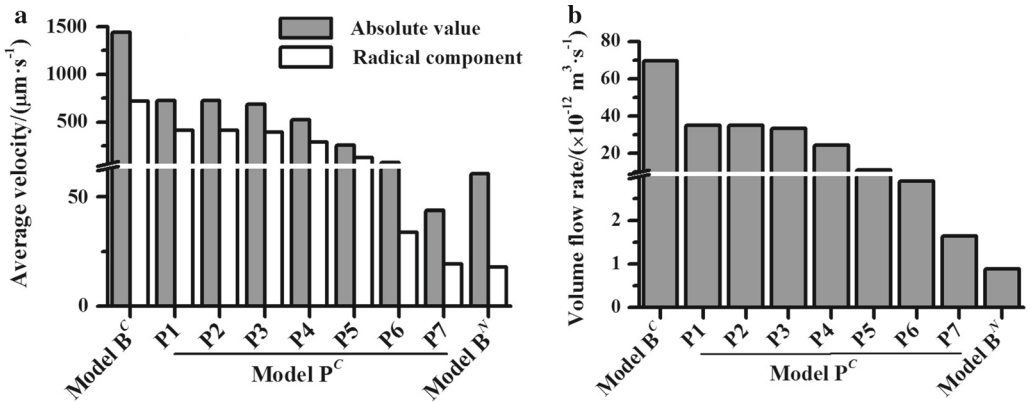

Fig. 3 Effect of different PT permeability on average velocity (**a**) and volume flow rate upon (**b**) Model P for cirrhotic lobules (shortened as Model P^C). Also presented were those data from Model B in normal (Model B^N) or cirrhotic (Model B^C) lobules for comparison

Table 3 Experimental data compared with the models used in this work

Parameters	Value	Species	Source
Blood velocity ($\mu m \cdot s^{-1}$)	970 ± 430	Human liver with partial liver resection	[15]
	100–600	Normal rat liver	[16,34,37,38]
	490–560	Fibrotic rat liver	[16]
	510–2000	Cirrhotic rat liver	[16,37]
Volume flow rate ($m^3 \cdot s^{-1}$)	$(2.84-2.98) \times 10^{-13}$	Normal rat liver	[16]
	$(2.99-4.66) \times 10^{-13}$	Cirrhotic rat liver	[16]

B. This, in turn, presented localized high and low pressures around inlets and outlets of PTs and the CV, respectively (Fig. 4a), as well as reduced pressure gradient from PTs to the CV down to <5 Pa (Fig. 4b). Adding new vessels only in Model V was not able to alter the pressure profile significantly in contrast to that in Model B. Instead, it slightly decreased the pressure near the added vessels and reduced the pressure gradient between inlet and outlet down to 50 Pa (Fig. 4c, d). The simulations from Model P+V integrated both characteristics from Models P and V, yielding a pressure gradient between inlet and outlet down to 200 Pa (Fig. 4e) or between PT and CV up to 20 Pa (Fig. 4f).

Flow velocity profiles and volume flow rates were also revisited via the modified models. Average bulk velocity was reduced to different extents in all modified models compared to those from Model B (Fig. 4g). Specifically, the bulk velocity and its radical component from Model P decreased to be over two-fold higher than that in normal lobules (cf. Fig. 2g), which was similar to those from Model P+V. Adding collateral vessels in Model V alone was not able to reduce the velocities as effectively as in Model P and still yielded high values of >600 μm/s, while combining Model V with Model P (Model P+V) decreased the velocities moderately (Fig. 4g). Thus, enhancing PT resistance alone or together with adding collateral vessels could reduce the flow velocity in sinusoids.

Moreover, the change in volume flow rate using the modified models exhibited similar patterns with that of average velocities, as seen in Fig. 4h. Interestingly, the flow rate difference between cirrhotic lobules in Model P or P+V and normal lobules in Model B was reduced remarkably to be three- to five-fold, which was comparable with the flow rate difference reported experimentally [16] (Table 3). Adding collateral vessels in Model V slightly increased the flow rate out of the CV, as expected, but was not able to alter the flow rate around 7.5×10^{-11} $m^3 \cdot s^{-1}$ to that of Model B (Fig. 4h). Taken together, these analyses using modified models suggested that assigning a typical high resistance in PTs could better represent the pressure and flow velocity profiles, as well as estimate the volume flow rate in cirrhotic lobule.

3.3 Integrated analyses of pressure and flow patterns from PTs to CV

Prediction of blood flow dynamics between PTs and the CV in liver lobules is particularly crucial, not only because the localized flow governs the sinusoidal perfusion, but also because it is hard to determine the dynamics experimentally due to the small size of the observational targets. Thus, we further compared the pressure and flow patterns at an arbitrary radial line from the CV to PTs, i.e., a line at $Y = 0$, $Z = 0.125$ mm, inside liver lobules using all six models presented above. For the pressure pattern, the calculations obtained from this radical line also represented the pressure distribution observed from previous profiles (Fig. 5a). Specifically in cirrhotic lobules, assigning high resistance in PTs using Model P presented high pressure values with much less

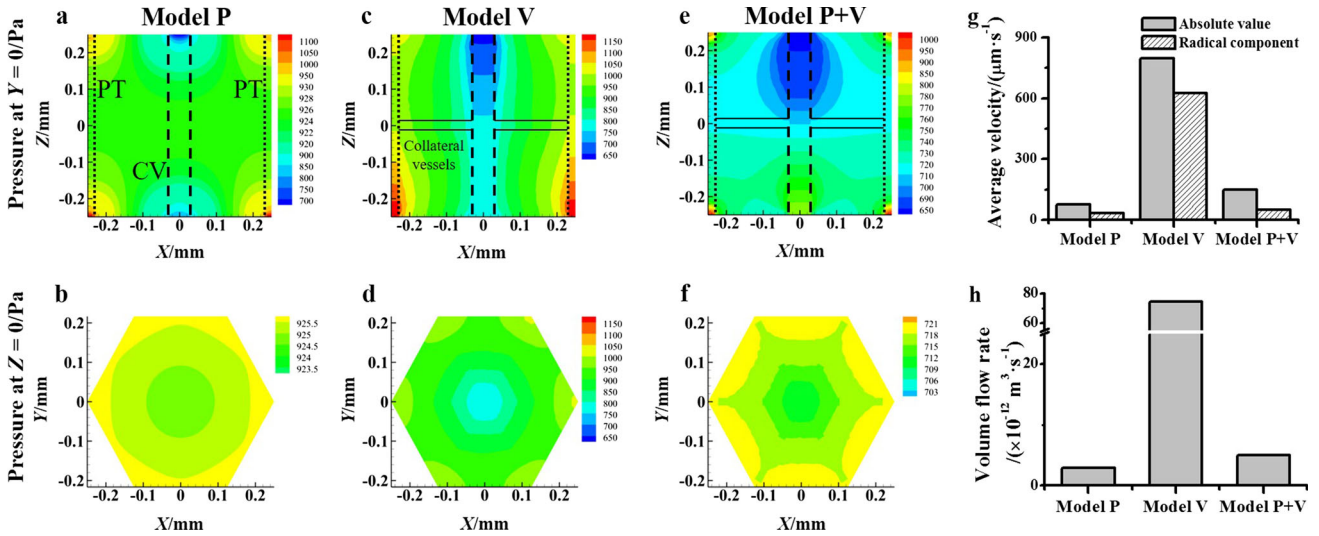

Fig. 4 **a–f** Pressure profiles at the planes of $Y = 0$ (**a**, **c**, **e**) and $Z = 0$ (**b**, **d**, **f**) in cirrhotic lobules using Model P (**a**, **b**), Model V (**c**, **d**) and Model P+ V (**e**, **f**). PTs, CV, and collateral vessels are illustrated as *dotted*, *dashed*, and *solid lines*, respectively. **g**, **h** Average velocities of absolute value and radical component (**g**) and volume flow rate (**h**) in sinusoidal zone were calculated. The permeability assigned for PTs in Models P and P+V was set as 10^{-13} m^2

fluctuation along the line (Fig. 5a, ☆). By contrast, combining high resistance in PTs with the added collateral vessels from PTs to the CV retained a stable pressure gradient along the line, which was also similar to that in normal lobules (Fig. 5a, □).

While a quite slow flow exists in the lobules and it is hard to apply the velocity nephogram for clarifying a small velocity difference, here we just compared the velocity distributions along this radical line (Fig. 5b). Specifically in cirrhotic lobules, local velocity along the line was found to be one order of magnitude higher than the basic cirrhosis model (Fig. 5b, ◇) and the modified collateral model (Fig. 5b, ▽) than those from the other four models. Clearly these predictions were not reasonable, since the experimental data only reads several tens and hundreds of micrometers per second [15,34] (Table 3). Meanwhile, a velocity peak at the vicinity of PTs or the CV appeared only in the two models with added collateral vessels (Fig. 5b, ▽ and □), presumably due to the alteration of the local flow field near PTs induced by adding the new vessels together with periodic boundary conditions at inlet and outlets. Since the single trajectory at a radical line may not be sufficiently representative, we proposed here that average bulk velocity could be a more reasonable basis by which to evaluate the reasonability of the developed models.

3.4 Interplay effect of flow direction between PTs and CV

Another issue is the diverse perfusion pattern inside a physiological lobule, since the blood in PTs can flow in either the same or the opposite direction as that in CV. While all the above modeling was conducted in a unified flow direction between PTs and CV, here we simply applied a basic Model B to test this impact. In a reverse flow direction, the pressure profiles obtained (Fig. 6a–f) were similar to those in a unified flow direction (Fig. 2a–f), as seen in the fluid flow from PT inlets to PT outlets and the pressure gradient from PTs to the CV in both cases. The main difference in these pressure profiles between the two direction settings lies in their specific patterns. Obviously, the opposite flow direction setting led to a reversed pressure gradient from PT inlets to PT outlets, as expected, and the pressure gradient from PTs to the CV then shifted to the opposite terminal. Meanwhile, average bulk velocity, radical velocity component, and volume flow rate presented similar patterns between the two settings (Fig. 6g, h), further confirming the reasonability of our modeling. Thus, these simple analyses proposed a basic idea on the impact of physiologically-relevant flow direction on lobule flow dynamics.

4 Discussion

In this study, we developed six 3D computational models of liver lobules for analyzing flow dynamics of three pathophysiological cases. Compared with those porous media theory-based models described previously [18,19,21,35], the novelty of our modeling lay in three aspects. First, we estimated, from murine lobule data, the pressure gradient between inlet and outlet of PT or CV for human lobules, figures which are not available experimentally. Second, different levels of high resistance in PTs were assigned using

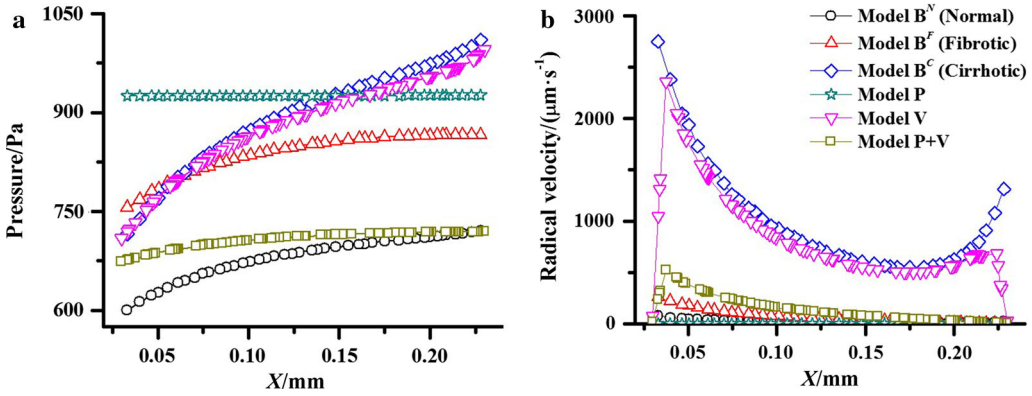

Fig. 5 Comparisons of pressure (**a**) or radial velocity (**b**) distribution along a typical line from CV to PT at $Z = 0.125$ mm at $Y = 0$, estimated from all the basic and modified models in normal, fibrotic, and cirrhotic lobules. Numerical simulations were conducted using varied pressure boundary conditions, porosity and permeability in Tables 1 and 2

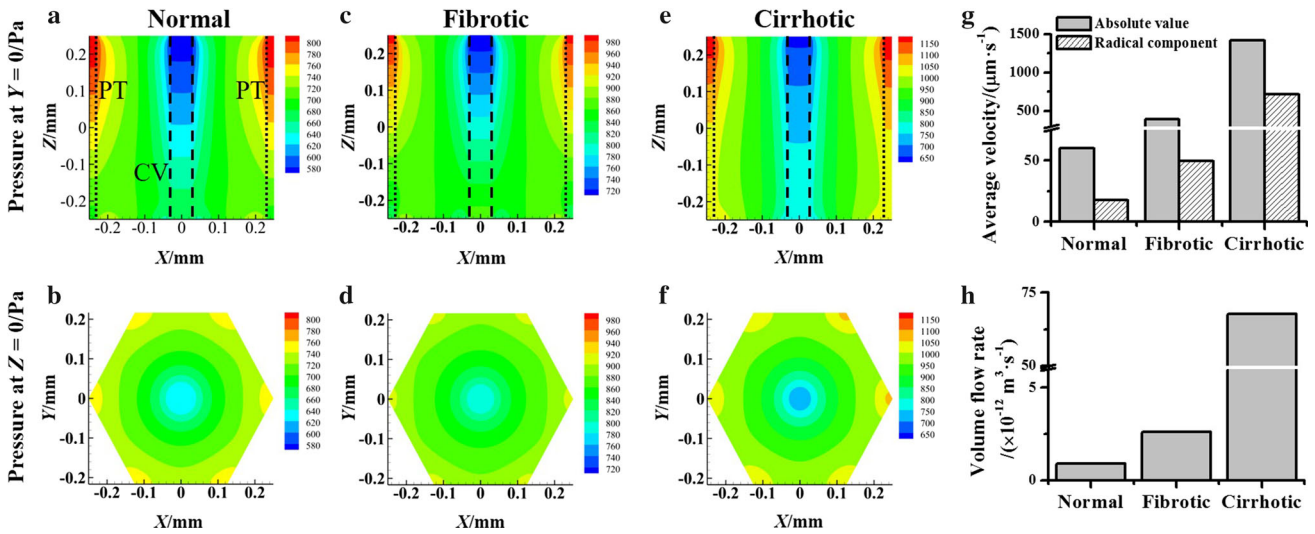

Fig. 6 **a**–**f** Pressure profiles at the planes of $Y = 0$ (**a**, **c**, **e**) and $Z = 0$ (**b**, **d**, **f**) in normal (**a**, **b**), fibrotic (**c**, **d**), and cirrhotic lobules (**e**, **f**) on Model B when the flow in PTs and CV yielded opposite directions. PTs and CV are illustrated as *dotted* and *dashed lines*, respectively. **g**, **h** Average velocities of absolute value and radical component (**g**) and volume flow rate (**h**) in sinusoidal zone were calculated using the same parameter setting as those in Fig. 2, except that the flow direction in PTs was reversed with regard to that in the CV

porous media theory, attempting to mimic the pathological progress from normal to fibrotic and then to cirrhotic lobules. Third, collateral vessels between PTs and the CV were added alone or together with high resistance in PTs, trying to replicate the actual sinusoidal perfusion in vivo. From these models, our analyses indicated that the approximations of ordinary flow for PTs and the CV and of porous media for the sinusoidal network are reasonable only for normal or fibrotic lobules. The features of high resistance in PTs and multiple shunts between PTs and the CV should be taken into consideration for describing the flow dynamics in cirrhotic lobules.

Comparing the pressure difference inside normal, fibrotic, and cirrhotic lobules for human liver is difficult, since no experimental data at the terminal portal vein and hepatic artery or vein are available. Fortunately, data from murine liver lobules are available, enabling us to estimate the pressure gradient between inlet and outlet in human lobules required for flow dynamics analysis. Here we simply assumed that this pressure difference was comparable between murine and human lobule to set up the relevant pressure boundary conditions. This setting is mainly attributed to the consistent periodic change of blood flow in arteries among distinct mammalian species [29]. In fact, the similarity of blood flow in mammals represent the propagation of pulse waves along length-varied blood vessels, and the bioindicator and biomass usually obey a power law with a different power component [36]. Unfortunately, it is very unclear about this power law for pressure distribution in the circulatory system due to its diversity and complexity. Thus, as the first step, we just obtained the pressure gradient ratio between fibrotic or cirrhotic to normal lobules from murine data and applied it to estimate the value for humans. In this

regard, it is not meaningful to compare the pressure values between the measurements and the conditions used in the calculations. Instead, how high resistance in PTs and collateral vessels between PTs and the CV alter the pressure profile in fibrotic or cirrhotic lobules is a key issue when applying these models. The resulted simulations profiled the impact of the two factors independently or cooperatively (Figs. 2a–f, 4a–f, and 6a–f). Pathologically in cirrhotic livers, severe portal occlusion induces high resistance in the liver organ and the occurrence of collateral vessels relaxes high pressure in the portal vein region, which is consistent with the predictions presented here.

Flow velocity calculated here was consistent with those measured in the literature. Our simulations from all six models indicated that the average bulk velocity and its radical component read from several tens to a thousand micrometers per second (Figs. 2g, 3a, 4g). Specifically, the bulk velocity was $0-500\,\mu m/s$ for normal lobules, high resistance cirrhotic lobules (Model P) and high resistance cirrhotic lobules with collateral vessels (Model P+V), which are consistent with those measured in murine sinusoids ($0-400\,\mu m/s$) [16,37,38] and in human liver ($\sim$1 mm/s) [15] (Table 3). Thus, the predictions from the current modeling are reasonable and meaningful, especially when considering that it is hard to measure the flow velocity inside human liver lobules.

In addition to pressure gradient and flow velocity, volume flow rate is another key dynamics parameter, which is not only used to validate the modeling but also serves as one of the clinical criteria in diagnosing liver diseases. It is known experimentally that the flow rate in murine cirrhotic lobules is enhanced about two-fold [16] (Table 3). Measured data for cirrhotic human livers are quite diverse, that is, the flow rate in the whole liver organ can either be enhanced [39] or be reduced [40] within a factor of two. We also note that the data for human liver lobule are not available due to the technical difficulties of noninvasive or minimally invasive surgery. Comparing our predictions with those existing data, it was evident that our basic models were not reasonable, at least in estimating the flow rate in cirrhotic livers. Modifying the models by assigning high resistance in PTs significantly improved the reasonability of our modeling in this regard. Together with high pressure profiles observed (Fig. 4a–f), this modified model is also pathologically relevant since the high flow resistance at the terminal vessels and ducts is one of the causes for the occurrence and progress in cirrhotic livers. Specifically, we also compared or estimated this flow rate value for murine and human livers. In normal lobules, both measured and calculated values are in the same order of magnitude of 10^{-11}–10^{-12} $m^3 \cdot s^{-1}$ for murine (Figs. 2h, 3b, 4h, and Table 3). For the human liver, assuming that the density of liver parenchyma is similar to that of water, the volume of the entire liver organ reads about 1000−1500 ml based on its mass of 1.0−1.5 kg [39,41]. This turns out to be the total $(0.82-1.24) \times 10^7$ lobules upon the dimension given in the current work. Thus, the flow rate per lobule is estimated to be $(1.35-2.02) \times 10^{-12}$ m^3/s, which is similar to (slightly higher than) the value from our simulations. In cirrhotic lobules, the flow rate is found to be increased or decreased only a half using the data from entire liver organ, while it reads three- or five-fold enhancement from the simulations based on the modified models for an individual lobule. These remarkable differences between the measurements and the calculations are mainly due to the parameter setting in the calculations, which can be easily optimized in the future applications of these models to specific diseases. Nevertheless, our modeling provides a reasonable platform by which to analyze the volume flow rate inside liver lobule.

Collectively, the validity of these computational models, especially for cirrhotic lobules, was embodied in the following three aspects: first: the pressure profiles were consistent with experimental data. High resistance in PTs and high pressure within whole lobule were presented with small pressure gradient from PTs to the CV in Model P (Fig. 4a, b). Moreover, the appearance of adaptive shunts was favorable to releasing high pressure and decreasing the pressure gradient in Model P+V (Fig. 4e, f). Second, the differences of average velocity between normal and fibrotic or cirrhotic lobules presented here (Figs. 2g, 4g) were comparable with the experimental data [16] (Table 3). Third, the well-matched volume flow rate between modeling prediction and experimental data further validated the models (Figs. 2h, 4h). Furthermore, the predicted pressure gradient and flow velocity profiles could also serve as input flow conditions when attempting to elaborate flow features of a single sinusoid [42] or could even elucidate the flow-induced cell-cell interactions within sinusoids.

In conclusion, we developed six effective 3D computational models for quantifying the flow dynamics mainly in cirrhotic liver lobules. Pressure and flow velocity profiles and volume flow rates were analyzed and the resulted predictions were comparable with existing experimental data. This modeling is meaningful when considering the technical difficulties in defining the local flow field experimentally and the complexity in promoting high resistance and collateral vessels with the progression of cirrhosis. This work furthered our understanding of the flow dynamics among normal, fibrotic, and cirrhotic lobules.

Acknowledgements This work was supported by the National Natural Science Foundation of China (Grants 31230027, 91642203, and 31661143044) and the Frontier Science Key Project of Chinese Science Academy (Grant QYZDJ-SSW-JSC018).

References

1. Wong, J., Johnston, B., Lee, S.S., et al.: A minimal role for selectins in the recruitment of leukocytes into the inflamed liver microvasculature. J. Clin. Invest. **99**, 2782–2790 (1997)

2. Li, N., Lu, S.Q., Zhang, Y., et al.: Mechanokinetics of receptor-ligand interactions in cell adhesion. Acta Mech. Sin. **31**, 248–258 (2015)
3. Sato, Y., Tsukada, K., Hatakeyama, K.: Role of shear stress and immune responses in liver regeneration after a partial hepatectomy. Surg. Today **29**, 1–9 (1999)
4. Monga, S.P.S.: Molecular Pathology of Liver Diseases. Springer Science & Business Media, Berlin (2011)
5. Schuppan, D., Afdhal, N.H.: Liver cirrhosis. Lancet **371**, 838–851 (2008)
6. Tsochatzis, E.A., Bosch, J., Burroughs, A.K.: Liver cirrhosis. Lancet **383**, 1749–1761 (2014)
7. Rappaport, A., Borowy, Z., Lougheed, W., et al.: Subdivision of hexagonal liver lobules into a structural and functional unit. Role in hepatic physiology and pathology. Anat. Rec. **119**, 11–33 (1954)
8. Kiernan, F.: The anatomy and physiology of the liver. Philos. Trans. R. Soc. Lond. **123**, 711–770 (1833)
9. Debbaut, C., Vierendeels, J., Casteleyn, C., et al.: Perfusion characteristics of the human hepatic microcirculation based on 3D reconstructions and computational fluid dynamic analysis. J. Biomech. Eng. **134**, 011003 (2012)
10. Bataller, R., Brenner, D.A.: Liver fibrosis. J. Clin. Invest. **115**, 209–218 (2005)
11. Sharma, M., Rameshbabu, C.S.: Collateral pathways in portal hypertension. J. Clin. Exp. Hepatol. **2**, 338–352 (2012)
12. Groszmann, R.J., Glickman, M., Blei, A.T., et al.: Wedged and free hepatic venous pressure measured with a balloon catheter. Gastroenterology **76**, 253–258 (1979)
13. Yzet, T., Bouzerar, R., Baledent, O., et al.: Dynamic measurements of total hepatic blood flow with Phase Contrast MRI. Eur. J. Radiol. **73**, 119–124 (2010)
14. Genzel-Boroviczény, O., Strötgen, J., Harris, A.G., et al.: Orthogonal polarization spectral imaging (OPS): a novel method to measure the microcirculation in term and preterm infants transcutaneously. Pediatr. Res. **51**, 386–391 (2002)
15. Puhl, G., Schaser, K.D., Vollmar, B., et al.: Noninvasive in vivo analysis of the human hepatic microcirculation using orthogonal polorization spectral imaging. Transplantation **75**, 756–761 (2003)
16. Nakata, M., Nakamura, K., Koda, Y., et al.: Alterations to hepatic microcirculation in thioacetamide-induced cirrhotic livers of rats. Osaka City Med. J. **48**, 1–8 (2002)
17. Shibayama, Y., Nakata, K.: Localization of increased hepatic vascular resistance in liver cirrhosis. Hepatology **5**, 643–648 (1985)
18. Bonfiglio, A., Leungchavaphongse, K., Repetto, R., et al.: Mathematical modeling of the circulation in the liver lobule. J. Biomech. Eng. **132**, 111011 (2010)
19. Debbaut, C., Vierendeels, J., Siggers, J.H., et al.: A 3D porous media liver lobule model: the importance of vascular septa and anisotropic permeability for homogeneous perfusion. Comput. Method. Biomec. **17**, 1295–1310 (2014)
20. Eringen, A.C.: Continuum Physics. Vol III: Mixtures and Em Field Theories. Academic Press, London (1976)
21. Ricken, T., Dahmen, U., Dirsch, O.: A biphasic model for sinusoidal liver perfusion remodeling after outflow obstruction. Biomech. Model. Mechanobiol. **9**, 435–450 (2010)
22. Rani, H.P., Sheu, T.W., Chang, T.M., et al.: Numerical investigation of non-Newtonian microcirculatory blood flow in hepatic lobule. J. Biomech. **39**, 551–563 (2006)
23. Lettmann, K.A., Hardtke-Wolenski, M.: The importance of liver microcirculation in promoting autoimmune hepatitis via maintaining an inflammatory cytokine milieu-a mathematical model study. J. Theor. Biol. **348**, 33–46 (2014)
24. Rezania, V., Coombe, D., Tuszynski, J.A.: A physiologically-based flow network model for hepatic drug elimination III: 2D/3D DLA lobule models. Theor. Biol. Med. Modell. **13**, 1–22 (2016)
25. Wambaugh, J., Shah, I.: Simulating microdosimetry in a virtual hepatic lobule. PLoS Comput. Biol. **6**, e1000756 (2010)
26. Nishii, K., Reese, G., Moran, E.C., et al.: Multiscale computational model of fluid flow and matrix deformation in decellularized liver. J. Mech. Behav. Biomed. Mater. **57**, 201–214 (2016)
27. Peeters, G., Debbaut, C., Cornillie, P., et al.: A multilevel modeling framework to study hepatic perfusion characteristics in case of liver cirrhosis. J. Biomech. Eng. **137**, 051007 (2015)
28. Maass-Moreno, R., Rothe, C.F.: Distribution of pressure gradients along hepatic vasculature. Am. J. Physiol Heart. C **272**, H2826–H2832 (1997)
29. Noordergraaf, A., Li, J.K.-J., Campbell, K.B.: Mammalian hemodynamics: a new similarity principle. J. Theor. Biol. **79**, 485–489 (1979)
30. Yoneda, M., Yoneda, M., Mawatari, H., et al.: Noninvasive assessment of liver fibrosis by measurement of stiffness in patients with nonalcoholic fatty liver disease (NAFLD). Dig. Liver Dis. **40**, 371–378 (2008)
31. Dixon, J.B., Bhathal, P.S., O'brien, P.E.: Nonalcoholic fatty liver disease: predictors of nonalcoholic steatohepatitis and liver fibrosis in the severely obese. Gastroenterology **121**, 91–100 (2001)
32. Schiff, E.R., Sorrell, M.F., Maddrey, W.C.: Schiff's Diseases of the Liver. Lippincott Williams & Wilkins, Philadelphia (2007)
33. Hubscher, S.G., Burt, A.D., Portmann, B.C., et al.: MacSween's Pathology of the Liver. Elsevier Health Sciences, Amsterdam (2011)
34. Sturesson, C., Milstein, D.M., Post, I.C., et al.: Laser speckle contrast imaging for assessment of liver microcirculation. Microvasc. Res. **87**, 34–40 (2013)
35. Siggers, J.H., Leungchavaphongse, K., Ho, C.H., et al.: Mathematical model of blood and interstitial flow and lymph production in the liver. Biomech. Model. Mechanobiol. **13**, 363–378 (2014)
36. West, G.B., Brown, J.H., Enquist, B.J.: A general model for the origin of allometric scaling laws in biology. Science **276**, 122–126 (1997)
37. Koo, A., Liang, I.Y., Cheng, K.-K.: Effect of the ligation of hepatic artery on the microcirculation in the cirrhotic liver in the rat. Aust. J. Exp. Biol. Med. Sci. **54**, 287–295 (1976)
38. Macphee, P., Schmidt, E., Groom, A.: Intermittence of blood flow in liver sinusoids, studied by high-resolution in vivo microscopy. Am. J. Physiol. Gastrl. **269**, G692–G698 (1995)
39. Pan, Z., Wu, X.-J., Li, J.-S., et al.: Functional hepatic flow in patients with liver cirrhosis. World J. Gastroenterol. **10**, 915–918 (2004)
40. Shaldon, S., Chiandussi, L., Guevara, L., et al.: The estimation of hepatic blood flow and intrahepatic shunted blood flow by colloidal heat-denatured human serum albumin labeled with I131. J. Clin. Invest. **40**, 1346 (1961)
41. Dancygier, H.: Clinical Hepatology: Principles and Practice of Hepatobiliary Diseases. Springer Science & Business Media, Berlin (2009)
42. Du, Y., Li, N., Yang, H., et al.: Mimicking liver sinusoidal structures and functions using a 3D-configured microfluidic chip. Lab. Chip. **17**, 782–794 (2017)